ARRAY SHADING APPLIED TO BEAMFORMING TECHNIQUE FOR EVALUATION OF SLAT NOISE FROM -6° TO 18° ANGLES OF ATTACK

Filipe Ramos do Amaral, framaral@usp.br
Carlos do Carmo Pagani Junior, paganni@sc.usp.br
Fernando Henrique Tadashi Himeno, fernando.himeno@gmail.com
USP, SEA, Sao Carlos, Brazil, Zip Code 13566-590
Juan Carlos Serrano, jcserrano@unipamplona.edu.co
Universidad de Pamplona, Programa Ingeniería Mecánica, Pamplona, Colombia - Currently on leave for Doctoral Program at USP, SEA
Marcello Augusto Faraco de Medeiros, marcello@sc.usp.br
USP, SEA, Sao Carlos, Brazil, Zip Code 13566-590

Abstract. *This study focuses on investigating the slat noise of a two-dimensional scaled, unswept and untapered, MD30P30N high-lift model. The database refers aeroacoustic and aerodynamic measurements in a closed-section wind tunnel for a wide range of angles of attack, namely from -6° and 18°, and Mach number ranging from 0.07 to 0.1. Aeroacoustic measurements were carried using a wall-mounted microphone array. The signal processing applied to the acoustic data involved the conventional beamforming tecnique enhanced by an array shading based on the coherence between pairs of microphones. Two deconvolution algorithms, DAMAS and CLEAN-SC, are also part of the post-processing. Suction-based wall boundary-layer control was applied to provide a more two dimensional flow over the model span. Chord-wise and span-wise static pressure measurements were performed. Slat noise spectra revel low-frequency tones, broadband noise and a single broad tone in the higher frequency range. The results show all slat noise components are strongly affected by wing angle of attack. The low-frequency tones vanish at lower negative wing angles of attack but reach their higher level at lower positive angles of attack. Overall, the dominant part in the slat noise spectra reduces as the wing angle of attack increases, rendering higher frequency noise components potential contributors to the overall noise.*

Keywords: *high-lift devices, slat, aeroacoustic, beamforming, array deconvolution methods.*

1. INTRODUCTION

The substantial reduction in the turbofan noise emission achieved within the last decades rendered the airframe noise of large commercial aircrafts a potential contributor to their overall noise during approach and landing procedures, (CRIGHTON, 1991). Therefore, current endeavors aiming at silent aircrafts have been mostly focused on airframe noise reduction. Among airframe components, landing gears and high-lift systems, trailing-edge flaps and leading-edge slats, have been identified as prominent noise contributors, but their ranking depends on the aircraft model and high-lifts configuration, (DOBRZYNSKI, 2010).

During the aircraft approach and landing, the deployed leading-edge slats may span almost the entire wings, thus contributing to the overall noise emission as distributed noise sources, (GUO; YAMAMOTO; STOKER, 2003). For aircrafts of regional routes, the wing aspect ratio may be considered large regarding any other airframe component, rendering the slats the leading noise contributors. Slat noise has been studied from wind tunnel measurements, (KOLB et al., 2007; IMAMURA et al., 2009; MANOHA et al., 2012; PASCIONI; CATTAFESTA; CHOUDHARI, 2014; MURAYAMA et al., 2014), numerical simulations, (KHORRAMI; BERKMAN; CHOUDHARI, 2000; PASCHAL; JENKINS; YAO, 2000; TAKEDA et al., 2001; JENKINS; KHORRAMI; CHOUDHARI, 2004; LOCKARD; CHOUDHARI, 2011; SOUZA et al., 2015), and flyover tests, (CHOW; MAU; REMY, 2002). Wind tunnel experiments using scaled high-lift models have revealed a slat noise signature featuring from broadband to tonal noise components. Measurements using a swept and tapered wing produced slat noise spectra dominated by low-frequency multiple tonal peaks. Such tones were suppressed by tripping the boundary-layer at the slat lower surface, leading to broadband slat noise spectra, (DOBRZYNSKI et al., 1998). It is noteworthy to say that attempts of eliminating the tones by tripping the boundary-layer at the slat pressure surface of unswept and untapered high-lift models did not succeed, (KOLB et al., 2007; IMAMURA et al., 2009), or even led to an increase in the tones level, (MURAYAMA et al., 2014).

The results presented in this latter stem from aeroacoustic and aerodynamic measurements carried out in a closed-section wind using a two-dimensional *MD30P30N* high-lift model, (AMARAL et al., 2015; PAGANI; SOUZA; MEDEIROS, 2015b, 2015a). Acoustic data were recorded using a wall-mounted 62-elements microphone array. The array output was first processed with conventional beamforming and after post-processed using deconvolution techniques in order to enhance the quality of the results. Suction-based boundary-layer control was applied to ensure a more two-dimensional time-averaged flow over the wing model span. The acoustic database includes measurements for a wide range of wing angles of attack, namely from -6° to 18°, which was enough to provide a substantial variation in the *MD30P30N* slat noise signature.

From moderate to higher angles of attack, the higher frequency slat noise content is generally buried into the wind tunnel

background noise. At higher frequencies, a severe coherence loss may lead to a source level underestimate, (SIJTSMA, 2008). To improve the quantitative noise level information extracted from the array measurements, a strategy was adopted from which the microphone signals were weighted according to a coherence-based criterion. This is a simple but apparently original strategy aiming to improve the array gain for noise components that remain correlated among the array microphones after averaging a large number of data blocks. Its application to the experimental slat noise data led to an increase in the broad tone level of up to 3 dB, as well as an improvement in the quality of the recovered image source. Such results indicate that coherence loss may hinder aeroacoustic measurements even in a closed-section wind tunnels whether high-frequency noise source measurements are aimed.

The paper organized as follows. The section 2.presents a description of the experimental setup and measurement procedures. Section 3provides an overview about the phase-array methodology adopted to the acoustic database processing. In section 4.we discuss results for different airfoil angle of attack and flow speeds. The conclusions are summarized in section 5.

2. Experimental Setup

The geometry of *MD30P30N* high-lift airfoil model was the base for our experiments, 1. The model has a 500 mm chord in the stowed configuration and a 1300 mm span and is basically manufactured in aluminum alloy. Regarding the airfoil in the stowed configuration, the slat chord is $15\ \%$ and its gap and overlap are $2.95\ \%$ and $-2.50\ \%$, respectively, while the chord of the flap is $30\ \%$ and its gap and overlap are $1.27\ \%$ and $0.25\ \%$, respectively.

Figure 1: *MD30P30N* airfoil in deflected condition.

Experiments were conducted in a closed circuit wind-tunnel at Sao Carlos Engineering School (*USP-EESC*). The tunnel showed a closed test section of 1300 mm height, 1700 mm width and 3000 mm length and a contraction ratio of $1:8$. It was equipped with an axial fan driven by a 115 HP alternated current motor and could reach velocities up to 34 m/s. The angles of attack, AoA were based on the main element, between -6° and 18°. The free-stream speeds, U_∞, were 24, 27, 31 and 34 m/s, for all configurations. The wall boundary-layer was controlled through the application of suction upstream the slat and on he suction side of the main element for a better two-dimensional flow.

The model's instrumentation includes 146 static pressure tappings in the middle span along a chord-wise line, distributed on the slat, main element and flap and 42 static pressure tappings along the span in two positions on the suction side of the main wing, i. e., one placed near its leading edge and another near its trailing edge. Such 42 static pressure tappings monitored two-dimensionality of the time averaged flow over the model.

Boundary-layer suction was applied over the junction between the slat and the main element with wind-tunnel walls, aiming the correction of the model's effective angle of attack, i. e., to keep the flow around the model two-dimensional as possible. Such suction was applied with a frequency-controlled blower, and a previous study to determine the best frequency for each case, i. e., for each model's angle of attack and free-stream speed, was performed.

3. Acoustic Data Post-Processing

In-house codes implemented in frequency domain, including conventional beamforming technique, *DAMAS* (Deconvolution Approach for the Mapping of Acoustic Sources), (BROOKS; HUMPHREYS, 2006), and *CLEAN-SC* (CLEAN based on Source Coherence), (SIJTSMA, 2007), deconvolution methods were employed for the acoustical database post-processing. The acoustic beamforming algorithm applied assumes spherical waves propagation in a free field condition from a distribution of uncorrelated monopole point sources, (MUELLER et al., 2002; SARRADJ, 2012) . The cross-spectral matrix (*CSM*), of all sound pressure measurements of the array's microphones, is the first step for a beamforming estimate. For our codes, the *CSM* is calculated by segmenting the microphones time series into data blocks for the frequencies of interest and applying a windowing function (such as hanning window) over each block with $50\ \%$ data overlap. The Fast Fourier Transform (*FFT*) is then extracted and the outer product between pairs of microphones is evaluated. Some correction factors (owing to windowing function energy loss, wind tunnel-wall reflections and *FFT*) have been applied and the average over all blocks for each frequency is obtained. A scanning plan containing a discrete mesh of N points is defined around the assumed noise source region. The *CSM* is weighted with steering vectors stemmed from transfer functions that models at either frequency the sound propagation from each mesh focal point for all array microphones. This transfer function models the propagation of a pressure wave by accounting the phase delays and amplitude decay due to the spherical spreading of sound which travels between the source and the microphones. A spatial pressure level distribution can be achieved through a successive focusing of the array pattern on the target points of the scanning grid/mesh. Such a distribution indicates the most likely source position according to a contour level map, known as beamforming map or noise

source map, (MUELLER et al., 2002). Beamforming outputs are expected to provide almost the maximum response (peak) when a mesh focus point coincides with the actual position of the source. The following works provide more details about the data post-processing adopted by our research group, (PAGANI; SOUZA; MEDEIROS, 2015b; AMARAL et al., 2015).

Beamforming results, obtained in a conventional way, generate acoustic maps from the results provided by array's measurements. A phased-array output stems from the spatial convolution between the measured pressure field and the impulse-based array response. Due to finite spatial sampling and array aperture, which lead to limited array resolution and dynamic range, the beamforming map is biased by the array design and does not necessarily represent the actual source distribution. This drawback may be greatly remedied by a deconvolution between the measured sound field and the array pattern associated with a modeled distribution of sources. For *DAMAS* deconvolution method, (BROOKS; HUMPHREYS, 2006), statistically independent N sources are assumed for each mesh point as the array's pattern output - *psf* (point spread function). A linear system, with N unknowns, is set up in a way to connect the conventional beamforming output with its equivalent source distribution. On the other hand, *CLEAN-SC*, (SIJTSMA, 2007), aims at iteratively removing the part of the source plot on a conventional beamforming map, which is spatially coherent with the peak source, i. e., the main lobes are spatially coherent with their side lobes, as they originate from the same physical source. Therefore, the idea is to build a conventional beamforming map, find the main peak, then subtract the appropriately scaled point spread function (*psf*) from the map and finally replace the *psf* by a beam with no side lobes (already removed). This procedure is repeated for the find of sources and *cleaning* of the conventional beamforming map.

The post-processing parameters adopted in this study are described as it follows. The microphone signals were acquired over 39 s at a 51200 Hz sampling rate, by an array of 62 microphones, designed as a modified archimedean spiral. Frequencies were divided into narrow-bands with different resolutions along the frequency range of interest, therefore different lengths of data blocks were employed, as detailed in Tab. 1.

Frequency Range [kHz]	$0.50 - 1.60$	$1.65 - 3.20$	$3.30 - 6.40$	$6.60 - 12.80$	$13.20 - 25.20$
Frequency Resolution [Hz]	25	50	100	200	400
Length of Blocks	2048	1024	512	256	128

Table 1: Characteristics of Narrowband frequencies.

The array is wall-mounted in a position from which can be focused on the wing model's lower surface by a proper signal processing technique. A mesh sub-domain named region of interest, *ROI*, is defined for the evaluation of the noise spectra over array measurements. Figure 2 shows a schema of positions and dimensions of the mesh and *ROI* with respect to the model (projections of the slat, main element and flap on the array plan for model's 4° angle of attack) and the array. A study on how the slat center in horizontal (average measurement between leading and trailing edges projections over the array plan) and vertical (distance between array and the slat plans) directions changes between angles of attack in the -6° and 18° range was conducted for the setting of the *ROI*. With this study, a position was taken to center the domain and *ROI*, as 0.34 m from the array center at horizontal (span-wise) direction and 0.85 m from the array plane. The *ROI* dimensions are 800 mm in the span-wise direction and 180 mm in stream-wise direction. The spatial mesh used in the calculation of beamforming maps was contained in a rectangular domain with minimum dimensions of 1400 mm and 300 mm for the span-wise and stream-wise directions, respectively, centered at the slat geometrical center in a plan 850 mm away from the microphone's array. Domain dimensions, for the stream-wise and span-wise directions, are a function of the array's *beamwidth*, and their values are twice for the frequency of interest, until they have achieved the minimum values described above, when domain dimensions *lock* and do not depend anymore on the array's *beamwidth*. The grid spatial resolution (distance between neighboring points in an evenly spaced grid), was defined as a function of the given array *beamwidth* for each frequency of interest for the avoidance of spatial aliasing and promotion of more reliable reconstructions of complex sound source distributions, (BROOKS; HUMPHREYS, 2006).

When a microphone's array is placed outside of the wind-tunnel flow, mainly for open jet wind-tunnels and outdoor measurements (fly-over tests), a loss in the microphone's signal coherence is observed, mainly for higher frequencies. Such loss is due to the turbulent shear-layer the sound must cross, (DOUGHERTY, 2003; SIJTSMA, 2010; ERNST; SPEHR; BERKEFELD, 2015). For closed test section wind-tunnels and wall-mounted microphones array, the turbulence of the boundary-layer over the microphones shall be a source of coherence loss, therefore the spatial resolution of beamforming images and integrated sound levels show a poorer resolution. The microphones cross-spectra show lower intensity levels, as a consequence of the coherence loss caused by the flow turbulence level - even when *CSM* auto-spectra are discarded, the beamforming spatial resolution is much lower than that with no flow, (SIJTSMA, 2008). Another difficulty the microphone's array measurements face is the source directivity, a characteristic that can change according to the frequency. Therefore, the microphone's array may receive different signal patterns, depending on the frequency, and the beamforming codes may focus the source noise on a wrong geometrical region.

An array shading methodology, based on coherence between microphones signal measurements, was developed for improvements in the experimental results. Array shading methodologies for beamforming purposes are very common in the literature. Some authors, (CHRISTENSEN; HALD, 2004), use a weighting function applied to the steering vector

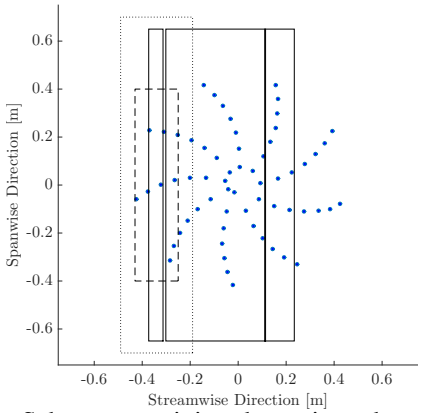

Figure 2: Domain and mesh parameters. Schema containing the region where the spatial distribution of noise sources were calculated (dashed lines), the mesh (dotted lines), the airfoil model at 4 ° angle of attack (continuous lines) and the microphone's array (filled circles).

component of conventional beamforming calculus for array dynamic range improvements. They used a Hamming window function over the array sensors at the cost of a poorer resolution measured by array *beamwidth*. It shall be recquired the *beamwidth* to be invariant under array's steering angle and frequencies, for providing a constant sensing area over noise source regions. A method for the achievement of such an invariant sensing area, which consists in shading the array sensors as a function of frequency, (HUMPHREYS et al., 1998), was developed. The authors also employed array shading techniques for the study of the jet noise, (BROOKS; HUMPHREYS; PLASSMAN, 2010). Shading methods are an option to correct the microphone density, therefore the acoustic power per unit area would be approximately constant, and also corrected the effective array's aperture due to the incoming sound coherence loss, (SIJTSMA, 2010).

The frequency domain beam-forming formulation used here to post-process wind tunnel acoustic data is given by

$$b\left(\vec{r}_s, \omega_l\right) = \boldsymbol{h}^{\dagger}\left(\vec{\boldsymbol{r}}, \omega_l\right) \boldsymbol{C}\left(\omega_l\right) \boldsymbol{h}\left(\vec{\boldsymbol{r}}, \omega_l\right), \tag{1}$$

in which $b\left(\vec{r}_s, \omega_l\right)$ is a squared pressure estimate obtained by algorithmically steering the array's beam toward a focal point located at $\vec{r}_s$ relative to a reference point, $\boldsymbol{o}$, on the array surface. The vector $\vec{\boldsymbol{r}}$ gathers all distances from the focal point to the array microphones. The cross-spectral matrix, $\boldsymbol{C}\left(\omega_l\right)$, contains all auto- and cross-spectra of the signals measured by the array, at frequency ω_l. The steering vector, $\boldsymbol{h}\left(\vec{\boldsymbol{r}}, \omega_l\right)$, is a complex-valued column vector modeling the wave field propagation from a point source at the focal point to each array microphone and the symbol $(\dagger)$ designates the Hermitian operator. The steering vector component for an arbitrary microphone of index m, or n, is herein given by

$$h_m\left(\vec{r}_m, \omega_l\right) = \frac{g_m\left(\vec{r}_m, \omega_l\right)}{\sqrt{\sum_{n=1}^{M}\sum_{m=1}^{M} \mid g_m \mid\mid g_n \mid}} \tag{2}$$

where M is the total number of microphones and $g_m\left(\vec{r}_m, \omega_l\right)$ is the transfer function $\left(1/r_m\right) e^{-i\omega_l(r_m)/c}$, modeling the sound wave received by the m-th array microphone due to a monopole source distant $r_m = \mid \vec{r}_m \mid$ from it, normalized by the transfer function modeling the sound wave received at the array reference point, $\left(1/r_s\right) e^{-i\omega_l(r_s)/c}$, which leads to

$$g_m\left(\vec{r_m}, \omega_l\right) = \frac{r_s}{r_m} e^{-i\omega_l(r_m - r_s)/c} \tag{3}$$

Eq. 3 holds for a situation where the medium, the source and the listener (microphone) are stationary relative to the same reference frame. In a wind tunnel, the microphones and sources are stationary while the flow filed drags the wavefront downstream, thus producing a convective sound effect that requires a proper correction to avoid misinterpretation of a source position. It was accomplished here by referring Eq. 3 to the effective distance the sound moves with respect to the medium, (OERLEMANS, 2009).

Inserting Eq. 2 into Eq. 1 and applying the required matrix products the beamformer spatial filter output writes as

$$b\left(\vec{r}_s, \omega_l\right) = \frac{\mid \sum_{n=1, n\neq m}^{M} \sum_{m=1, m\neq n}^{M} (g_m^*)[C_{m,n}](g_n) \mid}{\sum_{n=1, n\neq m}^{M} \sum_{m=1, m\neq n}^{M} \mid g_m \mid\mid g_n \mid}, \tag{4}$$

where the dependence on vector position and frequency was discarded for simplicity of notation and the symbol $(*)$ denotes complex conjugate. $C_{m,n}$ denotes the cross-spectrum between microphones labeled by m and n, and the condition $m \neq n$ means the cross-spectral matrix main diagonal elements have not been included in the summation. Eq. 4 shows the conventional beam-forming formulation as a weighted sum, in which the microphone cross-spectra are weighted by complex values, g_m^*, aiming at a proper signal phase delay and the output is scaled toward a reference level. Eq. 4 may potentially separate signal from different locations, thus behaving like a directional sound receiver whose performance is ultimately governed by the steering vector definition (SARRADJ, 2012) . If a grid of points is constructed to cover a region of interest for the mapping of acoustic sources, Eq. 4 may be applied to provide a source amplitude estimate at each grid point, thus generating a source image map at each spectral frequency, from which the level of distributed sources may be calculated by simple spatial integration, (BROOKS; HUMPHREYS, 1999).

In this study, an additional weighting factor w is introduced in the conventional beam-forming formulation according to

$$\boldsymbol{h}_w = \begin{bmatrix} h_1 w_1 \\ h_2 w_2 \\ \vdots \\ h_m w_m \\ \vdots \\ h_M w_M \end{bmatrix} \tag{5}$$

The weighting factor w_m for an arbitrary microphone of index m is defined as

$$w_m = \frac{1}{M-1} \sum_{n=1, n\neq m}^{M} \frac{[C_{m,n}]^2}{[C_{m,m}]\,[C_{n,n}]} \tag{6}$$

According to Eq. 6, w_m is the mean coherence of the m-th microphone signal with respect to the signals measured by the array microphones.

By inserting Eq. 5 into Eq. 4, the cross-spectra terms representing signals with high mean coherence level is to be over-weighted with respect to the non-weighted formulation, whereas otherwise under-weighted. The normalization adopted in Eq. 4 ensures the weighting factors do not lead to an array output gain by itself. As the the cross-spectral matrix results from averaging a large number of data blocks, this strategy is expected to increase the contribution from signals remaining highly correlated after the ensemble averaging, while reducing the contribution from poorly correlated signals.

4. Results and Discussions

4.1 Pressure Coefficient

Figure 3 show the distribution of the pressure coeficients, c_p, taken along the center-line of the model, in the chord-wise direction, and for two positions near the leading (upper curves) and trailing (lower curves) edges of the main element, in the span-wise direction. Such data were quantified for 34 m/s free-stream speed.

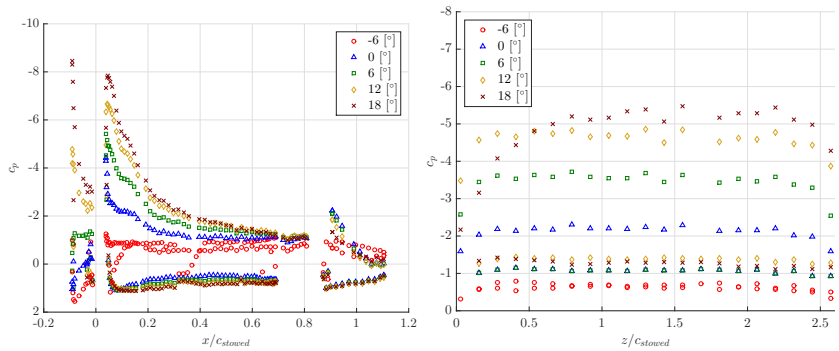

(a) (b)

Figure 3: Pressure coefficient, c_p. (a) Slat, Main Element and Flap chord-wise direction and (b) Main Element span-wise direction.

For lower angles of attack, as $-6°$, the circulation over the airfoil elements is ruined, whereas an increasing in the angle of attack increases the circulation. The main element and the slat are the airfoil elements most affected by the range of

angle of attack employed, due to their stronger suction peaks. Over the flap device, the circulation is almost not affected by the different slat configurations experimented. A better two-dimensionality in the span-wise direction was achieved for lower to mid angles of attack, as in the range of $0°$ to $12°$, due to lower circulation over the airfoil.

4.2 Preliminary Results

The nest study checked if the array coherence weighting methodology yields better results from the slat noise measurements. Figure 4 shows the noise spectra, including the post-processing with the *DAMAS* and *CLEAN-SC* deconvolution methods, *DAMAS* enhanced by coherence weighting and the wind-tunnel noise (noise spectrum with no model inside the wind tunnel). The figures also display two spectra related to the wind-tunnel noise case, evaluated for the same domain and *ROI* of the cases with a model inside the wind-tunnel, i. e., the *CSM* auto-spectra average and a beamforming calculus, with *DAMAS* deconvolution combined with the array coherence shading.

For lower angles of attack, as $-4°$, Fig. 4(a), the *CLEAN-SC* algorithm hardly found a noise source, therefore the noise spectra become impaired. On the other hand, for higher angles of attack, as $14°$, Fig. 4(c), the *CLEAN-SC* algorithm produced more intense noise, mainly for the broadband noise spectra component, than *DAMAS* (with and without array coherence shading applied). For moderated angles of attack, Figs. 4(b), and higher frequencies, *DAMAS* with array coherence shading detected noise spectra of more intense noise than the *CLEAN-SC* algorithm for some frequency ranges. The same can be inferred for the high-frequency broad tone, i. e., the hump/peak was highlighted when *DAMAS* with array coherence shading was employed.

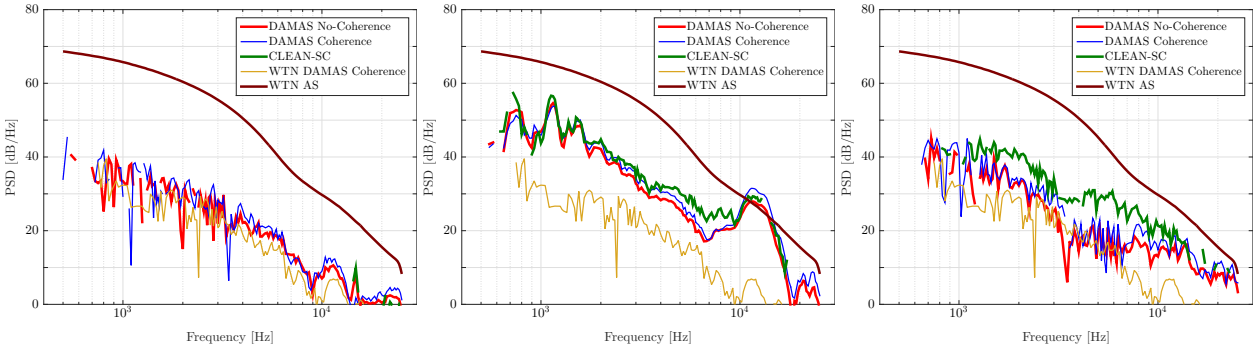

(a) (b) (c)

Figure 4: Comparison of noise spectra. U_∞ 34 m/s. AoA of (a) $-4°$,(b) $6°$ and (c) $14°$.

Source location maps, for a dynamic range of 12 dB/Hz, are shown in Fig. 5, for 34 m/s U_∞, and $2°$ angle of attack. Figure 5 shows a comparison among the conventional beamforming, *CLEAN-SC* and *DAMAS* (with and without array coherence shading applied) algorithms, that clarifies the suppression of side lobe levels characteristic of deconvolution methods. *CLEAN-SC* rebuilds the source location maps artificially, Fig. 5(b), therefore its maps do not show the line pattern expected for a slat source, punctual sources aligned are presented. Otherwise, as shown in Fig. 4, it can recover the noise spectra intensity. *DAMAS*, Fig. 5(c), enhances the beamforming technique ability of noise source maps reconstruction. It displays a reliable source map and when array coherence shading is applied, Fig. 5(d), such maps show better resolution and more intense noise.

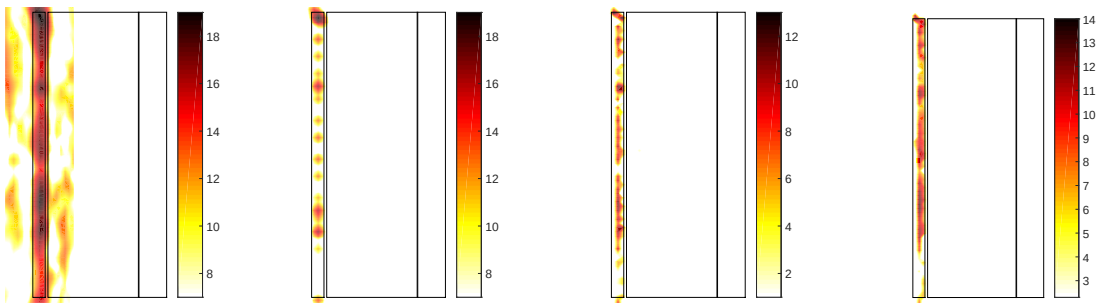

(a) (b) (c) (d)

Figure 5: Maps of noise sources. 34 m/s U_∞, $2°$ AoA, 10400 Hz. (a) Conventional beamforming, (b) CLEAN-SC and (c) DAMAS and (d) DAMAS Coherence.

After this study, the authors decided to apply *DAMAS* deconvolution with array coherence weighting to post-process the entire database and explore its results. This method reveals, in general, to rebuild best source location maps than

CLEAN-SC deconvolution, recovers higher noise spectra intensity especially at high frequencies, and is an adaptive method, choosing automatically, and based on the signal received and processed at *CSM*, which part, or cluster, of the array should be heavily weighted, i. e., which microphone is more coherent with the other ones on the array ones in average means.

4.3 Acoustic Database Results

Noise spectra results for *MD30P30N* are present in Fig. 6 for 34 m/s U_∞. Analyzing Figs. 4 and 6, noise spectra for lower angles of attack are of broadband like and its intensity levels are close to wind tunnel noise intensity level, with the last one estimated by beamforming calculus at the same domain and *ROI* of the *MD30P30N* cases were post-processed. Increasing the angle of attack, after $-2°$, slat noise components of multiple tonal peaks of low-frequency and high-frequency hump emerges, and so the slat noise became well characterized such as it is found on the literature, (DOBRZYNSKI; POTT-POLLENSKE, 2001; MENDOZA; BROOKS; HUMPHREYS, 2002; POTT-POLLENSKE; ALVAREZ-GONZALEZ; DOBRZYNSKI, 2003; KAEPERNICK; KOOP; EHRENFRIED, 2005; URA et al., 2010; TERRACOL; MANOHA; LEMOINE, 2011). For higher angles of attack, more than $10°$, the multiple tonal peaks of low-frequency component become suppressed and the broadband component overcomes, but in a lower intensity than when lower angles of attack. Baseline presents a high-frequency tonal around 15000 Hz and for more than $14°$ angle of attack. The authors believes that this spectral component may be spurious, consequence of a model imperfection that becomes important after $14°$ angle of attack.

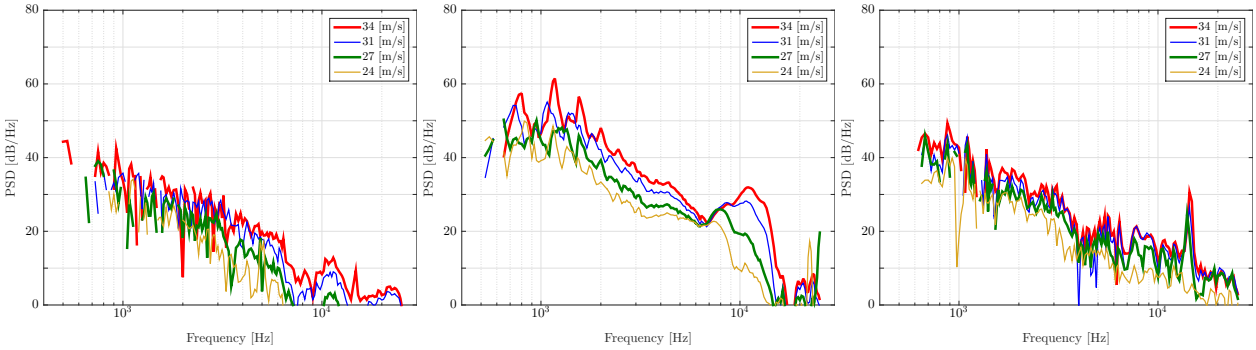

(a) (b) (c)

Figure 6: Noise Spectra. 34 m/s U_∞. AoA of (a) $-4°$, (b) $4°$ and (c) $18°$.

Mach and *Strouhal* collapses for all cases studied are shown in Fig. 7, with *Strouhal* number based on slat chord and free-stream speed and the spectra scaled by the $4th$ power of *Mach* number, which presents the best collapsing at vertical coordinate for these experiments. From low to mid angles of attack, between $-6°$ and $14°$, Figs. 7, all slat noise spectra components, multiple tonal peaks of low-frequency, broadband and high-frequency hump, shows reasonable collapse with *Mach* and *Strouhal* scale parameters. It is very clear that for lower angles of attack, Fig. 7(a), the slat noise spectra have almost the same intensity of wind tunnel noise. When higher angle of attack, Fig. 7(c), for high-frequency noise components there is no more collapse with *Strouhal* number, but with frequency, especially the high-frequency tonal. This collapse of the high-frequency tones with frequency, braces the hypothesis of such noise be of spurious nature.

Overall Sound Pressure Level (OASPL) over the frequency range of interest, for free-stream speed of 34 m/s, is present in Fig. 8 for all angles of attack and also for the wind tunnel noise. The maximum overall slat noise is at $0°$ of angle of attack, decreasing its intensity for lower and higher angles of attack.

5. Conclusion

An experimental aeroacoustic database for *MD30P30N* airfoil, post-processed with beamforming in-house codes, focusing on slat noise, was discussed on this paper for a wide range of angles of attack, in the range of $-6°$ and $18°$, and free stream speed between 24 m/s and 34 m/s. Suction wall boundary layer was performed aiming to provide a more two-dimensional distribution of pressure coefficient and to correct the effective angle of attack. Higher the angle of attack, worse the pressure distribution two-dimensionality over the main element suction side. Due to signal coherence loss, mainly for higher frequencies, and aiming the improvement of the quantitative noise level information extracted from the array measurement, an array shading methodology was developed in a way to outline this condition by weighting the microphones with the average coherence that it has with the other ones on the array for each frequency of interest. Both source location map and noise spectra presented improvements when comparing with the case without array shading - for slat noise, mainly broadband and high-frequency broad tone components spectra had an expressive benefit.

Analyzing the database, for lower angles of attack, less than $-4°$, the noise spectra is almost of broadband like - no multiple tonal peaks and high-frequency broad tone slat noise components are present - and its intensity is very close to the

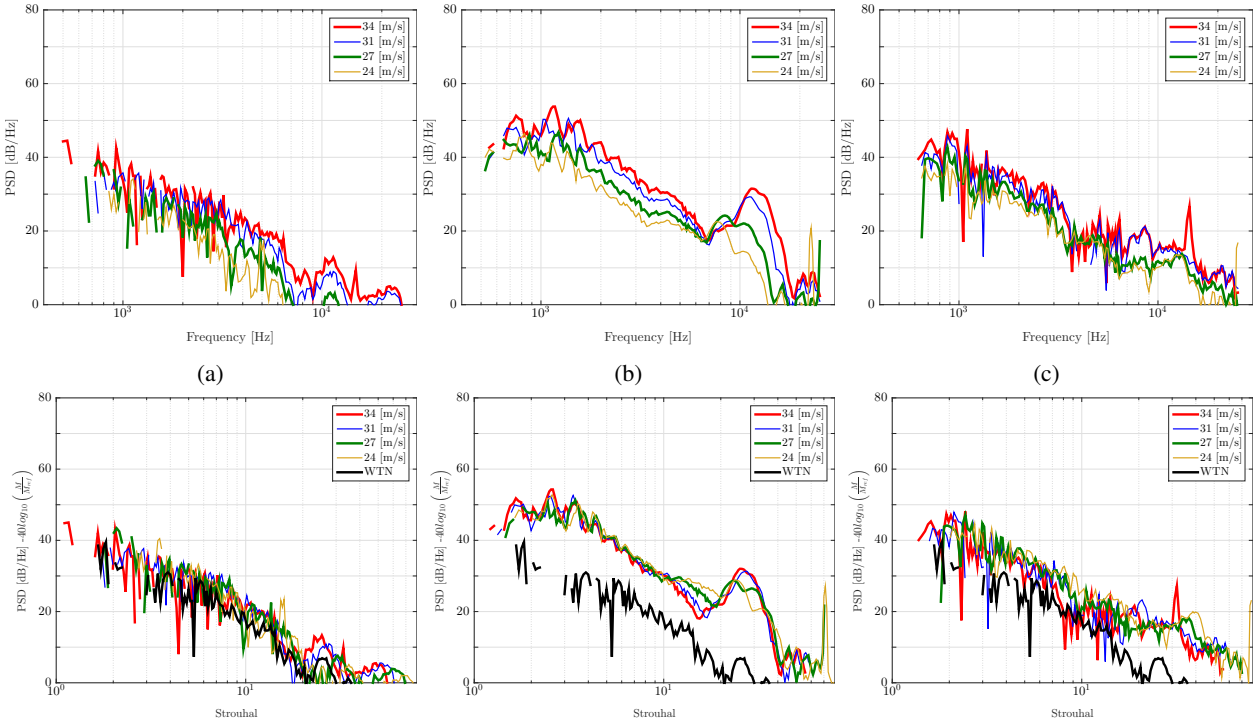

Figure 7: *Mach* and *Strouhal* Collapses. AoA of: (a) and (d) $-4°$, (b) and (e) $6°$ and (c) and (f) $16°$.

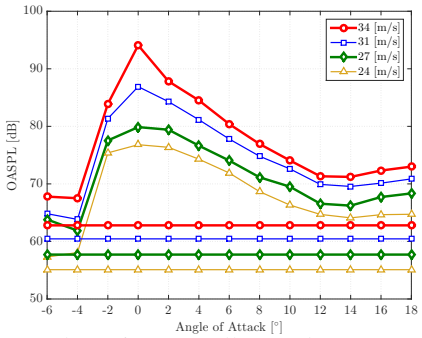

Figure 8: Slat noise Overall Sound Pressure Level.

wind tunnel noise one. For higher angles of attack, after $14°$, some high-frequency tones emerges, which is believed to be a model imperfection, due to these tones not scale with *Strouhal* number, but with frequency, for all free-stream speeds tested. The source location maps shows a punctual source on the slat at the frequency of these tones. When $0°$ of angle of attack, again some tonal noise emerges from slat noise broadband component and it is also believed to occur owing to a model imperfection, with the acoustic source maps presenting sparse sources all around the model. For moderated angles of attack, between $2°$ and $10°$, all three slat noise components, multiple tonal peaks of low-frequency, broadband and high-frequency broad tone, are well defined. Collapse with *Mach* number at fourth power has been found to fit better for this database. Overall noise shows that at $0°$ of angle of attack the spectra is the nosier one, while for negative and high positive angles of attack the overall level is closer to wind tunnel noise.

Array shading based on microphones coherence average reveals to be an alternative for slat noise characterization via beamforming technique. It presents a gain on spectra level for almost all frequency range studied, without decharacterizing the slat noise spectra component. Acoustic source maps become more uniform and its levels increases when comparing with the cases without any array shading. Although *CLEAN-SC* gives an excellent slat noise spectra presentation, it does not reconstruct the source maps of the quality that *DAMAS* is capable of doing. When coherence shading applied at beamforming formulation and employing *DAMAS* deconvolution, it is possible to ally a better slat noise spectra presentation with acoustic source maps of superior quality than *CLEAN-SC* is able to reconstruct.

6. ACKNOWLEDGEMENTS

F.R.A. received funding from CAPES/Brasil - Coordenação de Aperfeiçoamento de Pessoal de Nível Superior. F. H. T. H. received support from FAPESP/Brasil - Fundação de Amparo à Pesquisa do Estado de São Paulo. C. C. P., J. C. S. R. and M. A. F. M. received support from CNPq/Brasil - Conselho Nacional de Desenvolvimento Científico e Tecnológico. The authors would like to thank the project Silent Aircraft, which received funding from FAPESP/Brasil - Fundação de Amparo à Pesquisa do Estado de São Paulo.

7. REFERENCES

AMARAL, F. R. d. et al. Conference Paper, *Experimental Study of the Effect of a Small 2D excrescence placed on the Slat Cove Surface of an Airfoil on its Acoustic Noise*. American Institute of Aeronautics and Astronautics, 2015. Disponível em: <http://dx.doi.org/10.2514/6.2015-3138>.

BROOKS, T. F.; HUMPHREYS, W. M. Conference Paper, *Effect of directional array size on the measurement of airframe noise components*. American Institute of Aeronautics and Astronautics, 1999. Disponível em: <http://dx.doi.org/10.2514/6.1999-1958>.

BROOKS, T. F.; HUMPHREYS, W. M. A deconvolution approach for the mapping of acoustic sources (damas) determined from phased microphone arrays. *Journal of Sound and Vibration*, v. 294, n. 4-5, p. 856–879, 2006. ISSN 0022-460X. Disponível em: <<GotoISI>://WOS:000238359200011>.

BROOKS, T. F.; HUMPHREYS, W. M.; PLASSMAN, G. E. Conference Paper, *DAMAS Processing for a Phased Array Study in the NASA Langley Jet Noise Laboratory*. American Institute of Aeronautics and Astronautics, 2010. Disponível em: <http://dx.doi.org/10.2514/6.2010-3780>.

CHOW, L.; MAU, K.; REMY, H. *Landing Gears and High Lift Devices Airframe Noise Research*. American Institute of Aeronautics and Astronautics, 2002. Disponível em: <http://dx.doi.org/10.2514/6.2002-2408>.

CHRISTENSEN, J. J.; HALD, J. Report, *Technical Review: Beamforming*. 2004.

CRIGHTON, D. *Aeroacoustics of Flight Vehicles: Theory and Practice - Volume1: Noise sources*. [S.l.], 1991.

DOBRZYNSKI, W. Almost 40 years of airframe noise research: What did we achieve? *Journal of Aircraft*, v. 47, n. 2, p. 353–367, 2010. ISSN 0021-8669. Disponível em: <<GotoISI>://WOS:000276565300001>.

DOBRZYNSKI, W. et al. Conference Paper, *Airframe noise studies on wings with deployed high-lift devices*. American Institute of Aeronautics and Astronautics, 1998. Disponível em: <http://dx.doi.org/10.2514/6.1998-2337>.

DOBRZYNSKI, W.; POTT-POLLENSKE, M. Conference Paper, *Slat noise source studies for farfield noise prediction*. American Institute of Aeronautics and Astronautics, 2001. Disponível em: <http://dx.doi.org/10.2514/6.2001-2158>.

DOUGHERTY, R. Conference Paper, *Turbulent Decorrelation of Aeroacoustic Phased Arrays: Lessons from Atmospheric Science and Astronomy*. American Institute of Aeronautics and Astronautics, 2003. Disponível em: <http://dx.doi.org/10.2514/6.2003-3200>.

ERNST, D.; SPEHR, C.; BERKEFELD, T. Conference Paper, *Decorrelation of Acoustic Wave Propagation through the Shear Layer in Open Jet Wind Tunnel*. American Institute of Aeronautics and Astronautics, 2015. Disponível em: <http://dx.doi.org/10.2514/6.2015-2976>.

GUO, Y.; YAMAMOTO, K.; STOKER, R. Component-based empirical model for high-lift system noise prediction. *Journal of Aircraft*, v. 40, n. 5, p. 914–922, 2003.

HUMPHREYS, W. et al. Conference Paper, *Design and use of microphone directional arrays for aeroacoustic measurements*. American Institute of Aeronautics and Astronautics, 1998. Disponível em: <http://dx.doi.org/10.2514/6.1998-471>.

IMAMURA, T. et al. Conference Paper, *A Far-field Noise and Near-field Unsteadiness of a Simplified High-lift-configuration Model (Slat)*. American Institute of Aeronautics and Astronautics, 2009. Disponível em: <http://dx.doi.org/10.2514/6.2009-1239>.

JENKINS, L.; KHORRAMI, M.; CHOUDHARI, M. Conference Paper, *Characterization of Unsteady Flow Structures Near Leading-Edge Slat: Part I: PIV Measurements*. American Institute of Aeronautics and Astronautics, 2004. Disponível em: <http://dx.doi.org/10.2514/6.2004-2801>.

KAEPERNICK, K.; KOOP, L.; EHRENFRIED, K. Conference Paper, *Investigation of the Unsteady Flow Field Inside a Leading Edge Slat Cove*. American Institute of Aeronautics and Astronautics, 2005. Disponível em: <http://dx.doi.org/10.2514/6.2005-2813>.

KHORRAMI, M. R.; BERKMAN, M. E.; CHOUDHARI, M. Unsteady flow computations of a slat with a blunt trailing edge. *AIAA Journal*, v. 38, n. 11, p. 2050–2058, 2000. ISSN 0001-1452. Disponível em: <http://dx.doi.org/10.2514/2.892>.

KOLB, A. et al. Conference Paper, *Aeroacoustic Wind Tunnel Measurements on a 2D High-Lift Configuration*. American Institute of Aeronautics and Astronautics, 2007. Disponível em: <http://dx.doi.org/10.2514/6.2007-3447>.

LOCKARD, D. P.; CHOUDHARI, M. Conference Paper, *The Variation of Slat Noise with Mach and Reynolds Numbers*.

American Institute of Aeronautics and Astronautics, 2011. Disponível em: <http://dx.doi.org/10.2514/6.2011-2910>.
MANOHA, E. et al. Conference Paper, *Slat Noise Measurement and Numerical Prediction in the VALIANT Programme*. American Institute of Aeronautics and Astronautics, 2012. Disponível em: <http://dx.doi.org/10.2514/6.2012-2100>.
MENDOZA, J.; BROOKS, T.; HUMPHREYS, W. Conference Paper, *Aeroacoustic Measurements of a Wing/Slat Model*. American Institute of Aeronautics and Astronautics, 2002. Disponível em: <http://dx.doi.org/10.2514/6.2002-2604>.
MUELLER, T. J. et al. Book. *Aeroacoustic Measurements*. Berlin: Springer, 2002.
MURAYAMA, M. et al. Book Section, *Experimental Study on Slat Noise from 30P30N Three-Element High-Lift Airfoil at JAXA Hard-Wall Lowspeed Wind Tunnel*. American Institute of Aeronautics and Astronautics, 2014. (AIAA Aviation). Doi:10.2514/6.2014-2080. Disponível em: <http://dx.doi.org/10.2514/6.2014-2080>.
OERLEMANS, S. *Detection of aeroacoustic sound sources on aircraft and wind turbines*. Tese (Thesis) — University of Twente, 2009.
PAGANI, C. C.; SOUZA, D.; MEDEIROS, M. Experimental investigation on the effect of slat geometrical configurations on aerodynamic noise. *submitted to Journal of Sound and Vibration*, 2015.
PAGANI, C. C.; SOUZA, D.; MEDEIROS, M. Slat noise: aeroacoustic beamforming in closed-section wind tunnel with numerical comparison. *submitted to AIAA journal*, 2015.
PASCHAL, K.; JENKINS, L.; YAO, C. *Unsteady slat-wake characteristics of a high-lift configuration*. American Institute of Aeronautics and Astronautics, 2000. Disponível em: <http://arc.aiaa.org/doi/abs/10.2514/6.2000-139>.
PASCIONI, K.; CATTAFESTA, L. N.; CHOUDHARI, M. M. Book Section, *An Experimental Investigation of the 30P30N Multi-Element High-Lift Airfoil*. American Institute of Aeronautics and Astronautics, 2014. (AIAA Aviation). Doi:10.2514/6.2014-3062. Disponível em: <http://dx.doi.org/10.2514/6.2014-3062>.
POTT-POLLENSKE, M.; ALVAREZ-GONZALEZ, J.; DOBRZYNSKI, W. Conference Paper, *Effect of Slat Gap/Overlap on Farfield Radiated Noise*. American Institute of Aeronautics and Astronautics, 2003. Disponível em: <http://dx.doi.org/10.2514/6.2003-3228>.
SARRADJ, E. Three-dimensional acoustic source mapping with different beamforming steering vector formulations. *Advances in Acoustics and Vibration*, v. 2012, p. 12, 2012. Disponível em: <http://dx.doi.org/10.1155/2012/292695>.
SIJTSMA, P. Clean based on spatial source coherence. *International Journal of Aeroacoustics*, v. 6, n. 4, p. 357–374, 2007. Disponível em: <http://dx.doi.org/10.1260/147547207783359459>.
SIJTSMA, P. *Acoustic Array Corrections for Coherence Loss due to the Wind Tunnel Shear Layer*. 2008. Disponível em: <http://reports.nlr.nl:8080/xmlui/bitstream/handle/10921/278/TP-2008-112.pdf?sequence=1>.
SIJTSMA, P. *Phased array beamforming applied to wind tunnel and fly-over tests*. 2010. Disponível em: <http://papers.sae.org/2010-36-0514/>.
SOUZA, D. et al. Effect of an excrescence in the slat cove: Flow-field, acoustic radiation and coherent structures. *Aerospace Science and Technology*, v. 44, p. 108–115, 2015. ISSN 1270-9638. Instability and Control of Massively Separated Flows. Disponível em: <http://www.sciencedirect.com/science/article/pii/S1270963815000310>.
TAKEDA, K. et al. Conference Paper, *Unsteady aerodynamics of slat cove flow in a high-lift device configuration*. American Institute of Aeronautics and Astronautics, 2001. Disponível em: <http://dx.doi.org/10.2514/6.2001-706>.
TERRACOL, M.; MANOHA, E.; LEMOINE, B. Conference Paper, *Investigation of the unsteady flow and noise sources generation in a slat cove: hybrid zonal RANS/LES simulation and dedicated experiment*. American Institute of Aeronautics and Astronautics, 2011. Disponível em: <http://dx.doi.org/10.2514/6.2011-3203>.
URA, H. et al. Conference Paper, *Airframe noise measurements by using a simplified high-lift model*. 2010. 11 p. Disponível em: <http://www.icas.org/ICAS_ARCHIVE/ICAS2010/PAPERS/680.PDF>.

8. RESPONSIBILITY NOTICE

The authors are the only responsible for the printed material included in this paper.